

1 **Along arc heterogeneity in local seismicity across**  
2 **the Lesser Antilles subduction zone from a dense**  
3 **ocean-bottom seismometer network**

4  
5  
6 Lidong Bie\*, Andreas Rietbrock\*, Stephen Hicks, Robert Allen, Jon Blundy, Valerie  
7 Clouard, Jenny Collier, Jon Davidson, Thomas Garth, Saskia Goes, Nick Harmon, Tim  
8 Henstock, Jeroen van Hunen, Mike Kendall, Frank Krüger, Lloyd Lynch, Colin  
9 Macpherson, Richard Robertson, Kate Rychert, Stephen Tait, Jamie Wilkinson, Marjorie  
10 Wilson

11  
12 Corresponding author: Lidong Bie ([l.bie@liv.ac.uk](mailto:l.bie@liv.ac.uk))

13 Geophysical Institute, Karlsruhe Institute of Technology, Germany

14 \*Also at Department of Earth Ocean & Ecological Sciences, University of Liverpool, UK

15

16

17 **ABSTRACT**

18

19 The Lesser Antilles arc is only one of two subduction zones where slow-spreading  
20 Atlantic lithosphere is consumed. Slow-spreading may result in the Atlantic lithosphere  
21 being more pervasively and heterogeneously hydrated than fast-spreading Pacific  
22 lithosphere, thus affecting the flux of fluids into the deep mantle. Understanding the  
23 distribution of seismicity can help unravel the effect of fluids on geodynamic and  
24 seismogenic processes. However, a detailed view of local seismicity across the whole  
25 Lesser Antilles subduction zone is lacking. Using a temporary ocean-bottom seismic  
26 network we invert for hypocentres and 1-D velocity model. A systematic search yields a  
27 27 km thick crust, reflecting average arc and back-arc structure. We find abundant  
28 intraslab seismicity beneath Martinique and Dominica, which may relate to the  
29 subducted Marathon/Mercurius Fracture Zones. Pervasive seismicity in the cold mantle  
30 wedge corner and thrust seismicity deep on the subducting plate interface suggest an  
31 unusually wide megathrust seismogenic zone reaching ~65 km depth. Our results  
32 provide an excellent framework for future understanding of regional seismic hazard in  
33 eastern Caribbean and the volatile cycling beneath the Lesser Antilles arc.

34

35 **INTRODUCTION**

36

37 Subduction zones are key centers of mass transfer in the Earth, where the lithosphere  
38 and its cargo of volatiles are recycled back into the Earth's interior. In contrast to Pacific  
39 subduction margins, where fast-spreading lithosphere is consumed, subduction of slow-  
40 spreading lithosphere such as that formed in the Atlantic should result in a more  
41 heterogeneous distribution and possibly higher amount of fluids entering the subduction  
42 zone (Escartín *et al.*, 2008). The Lesser Antilles subduction zone in Eastern Caribbean  
43 is a global end-member in that the subducting plate is relatively old (~80 Myr) but yet  
44 subducts very slowly at ~19 mm/yr (DeMets *et al.*, 2010), and it is one of two zones  
45 where the slow-spreading Atlantic oceanic lithosphere is consumed. Along-arc changes  
46 in fluid flux might affect the distribution and character of seismicity and associated  
47 volcanism. For example, pore fluids within subducting sediments may affect the seismic

48 character of subduction megathrusts (Heuret *et al.*, 2012), and intermediate-depth  
49 intraslab earthquakes are probably caused by dehydration embrittlement (e.g., Abers *et*  
50 *al.*, 2006). A coherent view of local seismicity throughout the Lesser Antilles subduction  
51 zone is thus important for understanding fluid pathways and their influence on seismicity  
52 as well as for improving seismic hazard assessment.

53

54 Available measurements for the Lesser Antilles arc indicate that subduction parameters,  
55 such as slab dip (Wadge and Shepherd, 1984), Wadati-Benioff zone thickness, and slab  
56 geometry (Bie *et al.*, 2017), vary significantly along the Lesser Antilles subduction zone.  
57 Changes in slab dip as well as thickness and depth of the Wadati-Benioff zone near 15°  
58 latitude have been attributed to either the subduction of fracture zones (Schlaphorst *et*  
59 *al.*, 2016; Bie *et al.*, 2017) or a slab tear and gap wide enough to allow mantle flow  
60 through (e.g., van Benthem *et al.*, 2013; Harris *et al.*, 2018; Schlaphorst *et al.*, 2017). It  
61 is debated whether these changes in slab properties mark the location of the current  
62 North-South American plate boundary (Bie *et al.* 2017) or this boundary is located  
63 further north as suggested by plate reconstructions (Bird, 2003)

64

65 There have been several studies that characterise Lesser Antilles seismicity  
66 teleseismically (e.g., McCann and Sykes, 1984; Hayes *et al.*, 2013) as well as studies of  
67 local earthquakes for some parts of the arc (e.g., Dorel *et al.*, 1981; Paulatto *et al.*,  
68 2017; Ruiz *et al.*, 2013). These studies found higher rates of seismicity in the northern  
69 part of the Lesser Antilles subduction zone (14-18° N) than in the south, both in terms of  
70 small events and in historical records (e.g., McCann and Sykes, 1984; Hayes *et al.*,  
71 2013). Two historic  $M > 8$ , presumably thrust, earthquakes have been documented in the  
72 northern Lesser Antilles (e.g., Feuillet *et al.*, 2011). However, the strength of plate  
73 interface coupling and its variation along strike remain uncertain due to sparse GPS  
74 observations and slow convergence (e.g., López *et al.*, 2006). Local studies have  
75 detected earthquakes in the fore-arc corner of the mantle wedge (Ruiz *et al.*, 2013,  
76 Laigle *et al.*, 2013), something that has only been seen in a few subduction zones  
77 worldwide (e.g., Halpaap *et al.*, 2019).

78

79 No recent efforts have systematically characterised the distribution of small-magnitude  
80 seismicity along the full extent of the Lesser Antilles plate margin. The inherent nature  
81 of oceanic subduction zones means that onshore permanent seismometer networks  
82 have limited coverage and aperture, making it difficult to accurately locate small-to-  
83 moderate magnitude earthquakes in the back- and fore-arc. Furthermore, there is no  
84 well-constrained 1-D velocity model for the Lesser Antilles, which adds to earthquake  
85 location uncertainties. As part of our Volatiles Recycling in the Lesser Antilles (VoiLA)  
86 project (Goes *et al.*, 2019), we deployed a network of 34 broadband ocean-bottom  
87 seismometers (OBS) in 2016, which were recording for 14 months. We use this OBS  
88 data, complemented by recordings from permanent and temporal land stations, to jointly  
89 invert for 1-D P- and S-wave velocity models, earthquake locations and station  
90 corrections. Our study provides the first unified reference velocity model for the Lesser  
91 Antilles region, useful for the routine location of earthquakes in the area. The recorded  
92 seismicity provides the opportunity to understand the fore- and back-arc structure,  
93 thermal structure in the mantle wedge, and deformation mechanisms at intermediate  
94 depths in the subducted slab.

95

## 96 **SEISMIC EXPERIMENT AND DATA**

97

98 In March 2016, a network of 34 broadband OBS was installed across the fore- and  
99 back-arc regions of the Lesser Antilles subduction zone (Figure 1). The OBS were  
100 retrieved in May 2017. Two stations encountered hardware failures, leaving 32 stations  
101 with useable data (Goes *et al.*, 2019). In addition to our temporal OBS observations, we  
102 collected seismic data from existing permanent stations as archived by IRIS DMC  
103 (Figure S1). We also filled the gap in permanent stations along the southern end of the  
104 arc by deploying eight temporary stations in January 2017.

105

106 Multi-channel seismic surveys were also made during expedition JC149 in April 2017.  
107 Shooting occurred along eight lines, most of which were in a north-south direction along  
108 the arc and in the back-arc, with two lines taken perpendicular to the arc in the north of  
109 the subduction zone (Figure S1). These active-source data help to constrain the shallow

110 velocity structure of the subduction zone, an area poorly resolved in many passive-  
111 source tomographic inversions.

112

## 113 **MINIMUM 1-D VELOCITY MODEL**

### 114 **Initial Catalogue**

115 By collating the events reported by various agencies, we created an initial earthquake  
116 catalogue for manual picking P- and S-wave onset times. Our initial catalogue includes  
117 events from the online bulletin of the International Seismological Centre (ISC), the  
118 Martinique Seismic and Volcano Observatory, and the Seismological Research Centre  
119 of the University of West Indies (hereafter, UWI-SRC). We also detected additional  
120 events using an automated short-term average ratio/long-term average (STA/LTA)  
121 triggering algorithm (Nippres *et al.*, 2010) on vertical components of the ocean-bottom  
122 stations and performed an iterative event association procedure following Rietbrock *et*  
123 *al.* (2012). We then manually read P- and S-wave onset times from these potential  
124 events on the ocean-bottom stations and all available onshore stations using the  
125 Seismic Data Explorer (SDX) software (<http://doree.esc.liv.ac.uk:8080/sdx>). Based on  
126 onset time uncertainties, we assigned each observation a weight as follows: Weight 0  
127 (<0.1 s); Weight 1 (0.1-0.2 s); Weight 2 (0.2–0.5 s); Weight 3 (0.5–0.8 s); Weight 4 (>0.8  
128 s). Initial locations were computed using the IASP91 1-D reference velocity model  
129 (Kennett and Engdahl, 1991). This workflow resulted in a total of 502 confirmed  
130 earthquakes.

131

132 We computed local magnitudes ( $M_L$ ) for all events in our catalogue. Maximum  
133 amplitudes were taken from instrument-corrected waveforms, which were simulated to a  
134 Wood-Anderson seismometer. We took the largest peak-to-peak amplitude from all  
135 station components within a time window starting at the picked P-wave arrival and  
136 ending at a time window 30 seconds after the theoretical slowest travelling  $L_g$  wave  
137 (assuming a minimum  $L_g$  velocity of 3.0 km/s). We computed amplitudes for traces that  
138 had a root-mean square (RMS) signal-to-noise ratio greater than 3 to ensure that  
139 amplitude measurements were not contaminated by ocean microseism noise. We  
140 computed station magnitudes based on the  $M_L$  scale for central California (Bakun and

141 Joyner, 1984). Overall event magnitudes were then calculated based on a 25%  
142 trimmed-mean of station magnitudes to reject outliers. We found that station amplitudes  
143 measured at both ocean-bottom and onshore stations fit well the  $M_L$  scale over a range  
144 of hypocentral distance (see Figure S2 for examples). Regression analysis shows that  
145 our computed event local magnitudes correlate well with moment magnitude estimates  
146 for  $M_w > 4.5$  events (Figure S3a), and with local duration magnitudes ( $M_d$ ) for smaller  
147 events (Figure S3b).

148

### 149 **1-D minimum velocity model inversion**

150 Out of 502 manually picked events, we select a high-quality subset of 265 events with a  
151 maximum azimuthal gap of less than  $180^\circ$ , and with at least 20 P-wave and 5 S-wave  
152 arrivals. The subset consists of  $\sim 10,600$  P-wave and  $\sim 8,200$  S-wave arrivals for the  
153 simultaneous inversion of a 1-D layered velocity model, earthquake location and station  
154 corrections using the VELEST software (Kissling *et al.*, 1994).

155

156 The travel-time of a seismic wave is dependent on both the hypocentre parameters  
157 (origin time and location) and seismic velocity structure of the medium that the ray-path  
158 travels through. Such a coupled hypocentre-velocity problem can be solved by ray-  
159 tracing and updating the velocity model and hypocentre simultaneously (Kissling *et al.*,  
160 1988; Eberhart-Phillips, 1990; Thurber, 1992). We conducted the simultaneous  
161 inversion using the VELEST software by Kissling *et al.* (1994). VELEST requires that all  
162 stations must be in the same velocity layer. In this study, the deepest OBS station sits  
163  $\sim 5$  km below sea level and the greatest land station elevation is  $\sim 1.4$  km, making it  
164 impractical to set a model with a 7 km thick uppermost layer. Instead, we followed the  
165 strategy of Husen *et al.* (1999) and Hicks *et al.* (2014) by setting station elevations to  
166 zero and allowing station delay terms to absorb systematic travel-time errors due to  
167 elevation differences, as well as possible lateral heterogeneity in subsurface structure.

168

169 In addition to passive seismic data, we included 63 active shots from the seven shot  
170 lines (Figure 1) in order to better constrain seismic velocities at shallow depth,  
171 especially in the back-arc region, where few earthquakes with shallow hypocentral

172 depth occur. For each shot line, the gap between our selected neighbouring shots is  
173 roughly 15 km. The arrival times were manually picked on 22 OBS stations that record  
174 part of the 63 shots. The arrival times were corrected to subtract travel-time through the  
175 sea-water-column to be consistent with setting the station depth to sea level.

176

177 A robust initial starting velocity model is required as *a priori* information. We chose the  
178 velocity model computed by Raffaele (2011) as our starting model. Given that this  
179 model only extends to 30 km depth, we extended the starting model to a depth of 200  
180 km by merging it with the IASP91 velocity model below 30 km depth. To search for the  
181 best-fitting minimum 1-D model, ensuring that we are not fitting local misfit minima, we  
182 perturbed the starting model randomly within  $\pm 0.5$  km/s for all layers, resulting in 1000  
183 different synthetic starting models. The degree of convergence of the final velocity  
184 models from the 1000 inversions with different starting models is the first evidence of  
185 how robust the best-fitting model is. The velocity model that gives the minimum root-  
186 mean-square (RMS) misfit was taken as the optimal minimum 1-D velocity model.

187

188 We first invert for P-wave velocity model, using P-wave arrivals only. The best 10  
189 velocity models with the smallest RMS misfit converge very well. We notice an increase  
190 of velocity from 7.0 to 7.7 km/s at a depth of 27 km. To test whether the Moho depth can  
191 be constrained by our datasets, we manually alter the starting model by varying the  
192 depth to the bottom of the third layer from 21 to 37 km, in 2 km increments (Figure 2a).  
193 Then the inversion is conducted in the same way as described above by generating  
194 1000 variations of starting models for each Moho depth scenario and searching for the  
195 best model that gives minimum RMS. We then plotted the minimum RMS values versus  
196 the prescribed Moho depths, and the comparison shows a preferred average Moho  
197 depth of 27 km (Figure 2c).

198

199 After obtaining the best P-wave velocity model and optimal Moho depth, we  
200 subsequently inverted for S-wave velocity model using P- and S-wave arrival times.  
201 Similarly, 1000 variations of S-wave starting velocity model are generated, based on the  
202 P-wave velocity model and average  $v_p/v_s$  ratio derived from Wadati analysis. Due to the

203 trade-off between station corrections and the top layer velocity, we chose not to fix the  
204 top layer P-wave velocity as derived from the inversion.

205

## 206 **Characteristics of Minimum 1-D Velocity Model**

207 Tests with a range of starting models with various Moho dept (Figure 2a) result in the  
208 final minimum 1-D velocity model shown in Figure 2b. The best-fitting 1-D minimum  
209 velocity model comprises two layers of upper-plate crust underlying a top sedimentary  
210 layer. The estimated crustal P-wave velocity increases from 4.3 km/s at shallow depth  
211 to 7.7 km/s at 27 km depth. Affected by mostly near-vertical ray-paths, the uppermost  
212 crustal layer velocity is less well constrained, shown by poor convergence of the 10 best  
213 models, implying strong spatial variation of uppermost crustal velocity. This does not  
214 influence the final earthquake locations however, as our analysis of locations  
215 corresponding to the best 10 velocity models show a small average shift of <100 meters  
216 in all directions. The average velocities for the two main crustal layers are 6.3 km/s and  
217 7.0 km/s, consistent with those determined by Boynton *et al.* (1979) for the island arc.  
218 Our systematic search with varying crustal thickness yields a minimum misfit when the  
219 Moho depth is 27 km (Figure 2c). Crustal thicknesses derived by González *et al.* (2018)  
220 from surface wave and receiver function analysis under 19 land stations along the arc  
221 vary from 21 km beneath St Lucia to 33 km beneath Grenada in the south, with an  
222 average of 26 km (Figure 2c), which is similar to our model value even though this  
223 constitutes an average across the margin. Between 27 km and 200 km depth, the P-  
224 wave velocity ( $v_p$ ) and S-wave velocity ( $v_s$ ) increasing steadily to 8.7 km/s and 4.9 km/s,  
225 respectively, fits the observations (Table S1).

226

227 Station corrections are incorporated to compensate 3-D heterogeneity of near-surface  
228 velocity and station elevations. Station corrections for  $v_p$  are generally smaller than 0.5  
229 s, while for  $v_s$ , the station corrections are larger but mostly below 1.0 s (Figure 3). There  
230 are some systematic patterns, including positive corrections (i.e., thicker or slower crust)  
231 north and negative corrections south of reference station DP05 near Martinique in the  
232 central arc, as well as a linear correlation between station elevation and correction for



233 the OBS (Figure S4). Based on active source imaging (Allen *et al.*, 2019), our preferred  
234 interpretation is a systematic variation in crustal thickness from north to south.

235

## 236 **OVERALL CHARACTERISTICS OF LA SEISMICITY AND SUBDUCTION** 237 **GEOMETRY**

238

239 The best-fitting velocity model is used to relocate the original 502 manually-picked  
240 events. We conducted hypocentre location stability tests by randomly perturbing  
241 hypocentres  $\pm 7.5$ -12.5 km in 3-D, then relocating using the best-fitting 1-D velocity  
242 model (Figure 2b). When the azimuthal gap is less than  $\sim 270^\circ$ , the earthquakes  
243 generally relocate back to their original positions (Figure 4a), with a standard deviation  
244 of 0.21, 0.17, and 0.77 km for latitude, longitude and depth, respectively (Figure 4b). In  
245 addition to the azimuthal gap, we retained events that were relocated within 5 km depth  
246 variation from the original position. Strict filtering after hypocentre location stability tests  
247 resulted in 378 well-relocated events (Figure 5).

248

249 Although our observation period is short, the relocated seismicity exhibits a higher rate  
250 in the northern part of the subduction zone than in the south (Figure 5 and 6), consistent  
251 with previous studies (e.g., Bie *et al.*, 2017). Sparse seismicity is observed in the forearc  
252 region within 50 km distance from the trench. However, station coverage close to the  
253 trench in the outer forearc is very limited, so detection and location accuracy here is  
254 reduced. Most seismicity beneath the outer forearc is found in the north, where the  
255 forearc is less wide, and OBS stations were closer to the trench. We note that more  
256 smaller earthquakes may be found using template-matching techniques (e.g., Zhu *et al.*,  
257 2019). Here, we focussed on the larger events with robust arrival time determination,  
258 particularly for the generation of a well-constrained 1-D seismic velocity, with less  
259 emphasis on the evolution of seismicity in time and space.

260

261 Seismicity extends from the shallow upper crust of the overriding plate to intermediate  
262 depths of 180 km in the central slab (Figure 5). The distribution of seismicity with depth  
263 displays two peaks (see inset to Figure 5). Shallow seismicity increases with depth and

264 reaches its first peak at ~25 km, stays relatively high until there is a sharp reduction  
265 below ~60 km depth. At depths greater than ~80 km, seismicity increases again to  
266 depth of 170 km. The shallow peak comprises events in the overlying arc crust, and  
267 between about 25 and 60 km depth, events along the plate interface and in the mantle  
268 wedge corner. The deep peak consists of events within the subducting slab. The depth  
269 ranges of these peaks are similar to those that Paulatto *et al.* (2017) identified below  
270 Martinique, who proposed that the peaks in mantle wedge and slab seismicity are  
271 associated with slab dehydration around 40 and 150 km depth. In Section 5 we discuss  
272 the seismicity in each part of the system in detail.

273  
274 Our catalogue of regional seismicity provides new constraints on slab geometry. As  
275 shown in Figure 5, the seismicity distribution in this study does not agree well with the  
276 global Slab2 plate geometry model (Hayes *et al.*, 2018). The slab surface in Slab2 is up  
277 to 70 km shallower at depth of 180 km. Our seismicity is consistent with the  
278 teleseismically-constrained slab geometry of Bie *et al.* (2017) to ~80 km depth, while  
279 beyond that, seismicity in our study suggests a slightly steeper slab (profiles B-B', C-C',  
280 and D-D' in Figure S5). We thus integrated the local seismicity in this study with the  
281 global datasets used in Bie *et al.* (2017) and constructed a refined slab geometry  
282 (Figure 5). How the large difference in slab geometry affects geodynamic modelling and  
283 seismic hazard estimation will be a subject of a planned future study.

284

## 285 **DISCUSSION**

286

### 287 **Earthquakes in the Overriding Plate**

288 The shallow events lie in the overriding upper plate, reflecting fault failures in the fore-  
289 arc and/or are related to volcanic structures along the arc. Profile A-A' shows a cluster  
290 of events ~100 km westward of the trench at 14-25 km depth. These events are mostly  
291 aftershocks of the  $M_w$  5.7 thrust earthquake on 17 April 2017. The trenchward-dipping  
292 alignment of the cluster may indicate failure of a back-thrust fault bounding the western  
293 edge of the accretionary prism. A similar cluster can be found ~150 km west of the  
294 trench in profile B-B'. It is unclear whether this cluster on B-B' was on splay thrusts or

295 back-thrusts, given no clear alignment is shown and the relatively large RMS misfit  
296 values.

297  
298 Profile B-B' shows another cluster of shallow seismicity in line with the volcanic arc,  
299 between Guadeloupe and Dominica. This seismicity can be divided into two sequences.  
300 The first in 2016 starts with  $M_L$  4.5 and  $M_L$  4.1 events on 12 April, and lacks a clear  
301 subsequent aftershock sequence. The second sequence swarm started in April 2017  
302 denoted by a  $M_L$  3.5 earthquake (Table S2). Previously on 21 November 2004, this area  
303 experienced a  $M_w$  6.3 normal fault earthquake on the Roseau fault, which bounds the  
304 western side of the Les Saintes Graben between Guadeloupe and Dominica (Bazin *et*  
305 *al.*, 2010). The mainshock was followed by a long-lasting aftershock sequence on the  
306 Roseau Fault and a short-lived aftershock sequence on the smaller antithetic normal  
307 faults. Bazin *et al.* (2010) attributed the long-lasting aftershock sequence on the Roseau  
308 fault to this region being strongly faulted and filled with fluids, as inferred from a low  $v_p$   
309 anomaly and a high  $v_p/v_s$  ratio, while for the short duration aftershock sequence, fluid  
310 was less involved. This interpretation of high fluid content is consistent with our  
311 observation of occasional swarm activity in this region.

312  
313 Below Tobago, in the southern fore-arc, a sequence of aftershocks followed the  $M_w$  5.9  
314 strike-slip earthquake on 6 December 2016 (profile E-E' of Figure 5). Although, we  
315 expected these to be upper plate events, the aftershocks were relocated to ~60 km  
316 depth. A  $M_w$  6.1 earthquake with a similar faulting mechanism occurred on 2 April 1997  
317 at 45 km depth (NEIC), preceding a larger  $M_w$  6.7 normal fault earthquake on 22 April  
318 1997 at a much shallower depth of 5-15 km (NEIC). The GCMT focal mechanism for the  
319 2016 event suggests either sinistral strike-slip on an E-W striking sub-vertical (dip 67°)  
320 fault plane, or dextral strike-slip rupture on a near-vertical (80° dip) N-S striking fault  
321 (Figure 6). This mechanism is not consistent with the current active E-W dextral  
322 shearing across the Caribbean-South American plate boundary zone (e.g., Weber *et al.*,  
323 2015). These strike-slip events lie anomalously deep beneath the fore-arc, and the 2016  
324 cluster is close to the top of the subducting slab (profile E-E' of Figure 5). A likely

325 explanation is that the 2016 and 1997 strike-slip events ruptured structures within the  
326 down-going oceanic crust.

327

### 328 **Mantle Wedge Seismicity**

329 In addition to shallow upper crust activity, seismicity in the overriding plate appears in  
330 the mantle wedge corner above ~65 km depth and reaches into the lower crust (profiles  
331 in Figure 5), consistent with Ruiz *et al.* (2013) and Laigle *et al.* (2013). Seismicity in the  
332 mantle-wedge corner has implications for the thermal structure of the mantle wedge. It  
333 is normally assumed that the stable-unstable sliding transition in oceanic mantle occurs  
334 at temperatures of ~600°C (e.g., McKenzie *et al.*, 2005). By constructing an  
335 approximate curve delineating the wedge-shaped mantle corner seismicity, we found  
336 that the inferred transition consistently intersects the slab (red curve constrained by  
337 seismicity in Figure 5 profiles) at ~65 km depth across the subduction zone. In contrast  
338 to profiles in the north, the lack of mantle wedge seismicity in the EE' profile suggests  
339 that the mantle wedge temperature is different from north to south.

340

341 Mantle-wedge corner seismicity has been reported in only a few subduction zones  
342 around the world besides the Antilles, namely, NE Japan, New Zealand, Columbia and  
343 Greece. Such events have been attributed to the deformation of subducted seamounts  
344 (Uchida *et al.*, 2010), or hydraulic fracturing/fluid-assisted embrittlement or weakening  
345 due to the ascent of fluids from the slab (Chang *et al.*, 2017, Halpaap *et al.*, 2019). If  
346 this is the case for the Lesser Antilles, then the mantle wedge earthquakes may  
347 represent an unusual pathway for fluids driven off by early metamorphic reactions in the  
348 subducting plate. Alternatively, in a mantle wedge of mixed chemical composition  
349 (Laigle *et al.*, 2013), preferential hydration of the peridotite components may result in a  
350 differential volume change that may open fractures, causing extensional faulting in the  
351 mantle wedge (Iyer *et al.*, 2008).

352

### 353 **Plate Interface Seismicity**

354 In the north, interplate seismicity is observed from depths of about 10 km, while in the  
355 south, the shallowest seismicity is at 30 km depth at 14°N, and 45 km south of 12°N

356 (profiles in Figure 5). The largest thrust earthquake ( $M_w$  5.8) on the plate interface  
357 during our deployment occurred on 3 February 2017 east of Martinique. The Martinique  
358 earthquake was followed by aftershocks at  $\sim 50$  km depth (profile C-C'). We relocated  
359 the  $M_w$  5.8 mainshock to 51 km depth. The alignment of the sequence with the slab  
360 geometry indicates rupture of the plate interface and suggests a seismogenic zone  
361 reaching to at least 60 km depth, deeper than the fault locking depth of 5-25 km  
362 previously proposed by Smithe *et al.* (2015) using geodetic observations.

363  
364 The Martinique sequence occurred deeper than the intersection of the upper plate Moho  
365 ( $\sim 27$  km) with the down-going plate interface. This observation is similar to that found by  
366 Ruiz *et al.* (2013) of seismic activity offshore Martinique and Dominica, suggesting that  
367 the interplate seismogenic zone width is usually not limited by thickness of the upper  
368 plate crust, consistent with a global compilation by Heuret *et al.* (2011). However, the  
369 down-dip limit of  $\sim 65$  km depth that we find for the Lesser Antilles megathrust  
370 seismogenic zone is high compared to the global range of  $51 \pm 8$  km (Heuret *et al.*,  
371 2011). The Martinique sequence on the plate interface, together with supra-slab  
372 seismicity discussed in the previous section, suggest the existence of a cold mantle  
373 nose, which can effectively extend the decoupling depth of the slab and upper plate  
374 mantle (Wada and Wang, 2009). This wide seismogenic zone has important  
375 implications for the maximum magnitude of earthquakes that could occur in this region,  
376 and this may explain the large magnitudes of the Guadeloupe earthquakes in the  
377 1800s. An alternative to this is that this deeper part may represent seismic-aseismic  
378 transitional zone (e.g., Lay et al., 2012). Although large earthquakes may not initiate at  
379 this deeper depth, rupture may propagate into this region and effectively increase the  
380 earthquake magnitude and thus seismic hazard.

381

### 382 **Intermediate Depth Seismicity**

383 The Lesser Antilles Wadati-Benioff zone extends to 150-180 km depth with a  
384 concentration of intraslab seismicity beneath the center of the arc, between the islands  
385 of Guadeloupe and St. Lucia (Figure 5). During our experiment, a  $M_w$  5.6 earthquake  
386 occurred on 18 October 2016 southwest of Dominica at  $\sim 160$  km depth. This event had

387 a normal faulting mechanism with both nodal planes striking perpendicular to the arc,  
388 and in the direction of convergence. Normal faulting earthquakes are frequent within the  
389 slab at ~150 km depth between the islands of Dominica and Martinique, i.e. in the  
390 region with the densest intermediate depth seismicity. Similar recent moderate-to-large  
391 intraplate events (Figure 6) include a  $M_w$  5.6 on 28 December 2015, a  $M_w$  7.4 on 29  
392 November 2007, and a  $M_w$  5.8 on 24 September 1996 and an earlier magnitude 7.5 that  
393 occurred on 19 March 1953 (Stein *et al.*, 1983) ~100 km south of the 2016 event.  
394 According to the GCMT earthquake catalogue, all those events since the 1990s share a  
395 similar, normal faulting mechanism with a minor strike-slip component; at least one of  
396 the nodal planes strikes parallel with the subduction direction.

397  
398 Fault strikes parallel or oblique to the trench could be due to reactivation of subducted  
399 outer-rise normal faults formed at the mid-oceanic spreading ridge (e.g., Delouis and  
400 Legrand, 2007; Garth and Rietbrock, 2014). However, trench-perpendicular nodal plane  
401 ruptures cannot be explained in this manner. Instead, the intermediate-depth normal  
402 fault earthquakes mentioned above occurred around the projected positions of the  
403 subducted Marathon and Mercurius Fracture zones (Figure 6). This finding may suggest  
404 a link between the deep normal fault earthquakes and subducted fracture zones – which  
405 may be effective vessels to bring water to intermediate depths. Thus, the reactivation of  
406 inherited oceanic structures (e.g., fractures zones), facilitated by dehydration  
407 embrittlement, may be the dominant mechanism responsible for the normal faulting  
408 events seen at intermediate depth in the central arc. In other places along the arc,  
409 intermediate depth normal fault earthquakes are rare, which may suggest weaker  
410 hydration and smaller fluid fluxes, insufficient to drive significant dehydration  
411 embrittlement failure.

412

### 413 **Slab Tear?**

414 The coherent catalogue of seismicity compiled for this study offers a chance to test the  
415 hypothesis that a slab tear exists at 15°N - between the islands of Dominica and  
416 Martinique – as suggested by teleseismic tomography models and seismic anisotropy  
417 observations (Van Benthem *et al.*, 2013; Harris *et al.*, 2018; Schlaphorst *et al.*, 2017).

418 We projected seismicity in this area onto multiple profiles (with a 10 km gap between  
419 neighbouring profiles) perpendicular to the trench and marked those to the north of the  
420 profile in blue, and those to the south in red (Figure S6). This method can reveal the  
421 location of a slab tear, if two seismicity alignments with different dip angles are  
422 observed. Our results do not indicate any distinctive change in dip angle but rather a  
423 thickening of the Wadati-Benioff zone from north to south as shown by line 7 in Figure  
424 S6. The thickening here may define the northern boundary of the subducted Marathon  
425 Fracture zone. Seismicity during the period of our observation does not support the  
426 notion that a large-scale slab tear exists at this depth, but we cannot rule out a slab tear  
427 below the deepest seismicity.

428

## 429 **CONCLUSIONS**

430

431 In this study, we used seismic data from a dense OBS network to record local seismicity  
432 in the Lesser Antilles subduction zone and delineate changes in seismic deformation  
433 and velocity structure both with depth and along the arc. The joint inversion for a 1-D  
434 velocity model, earthquake location and station corrections yields an optimal crustal  
435 thickness of 27 km, representative of an arc-back-arc average. Abundant intermediate-  
436 depth seismicity is found beneath the islands of Martinique and Dominica, which may  
437 relate to the subducted Marathon and Mercurius Fracture Zones. Although a slab tear  
438 near 15°N has been proposed by previous teleseismic seismic studies, our seismicity  
439 distribution suggests thickening of the Wadat-Benioff zone, but without distinctive  
440 changes in the slab dip angle that would be expected for a tear. Interpretations of our  
441 earthquake locations reveal pervasive seismicity in the cold mantle wedge corner, which  
442 is not observed in many subduction zones. Together with the deep 2016 Martinique  
443 earthquake sequence on the plate interface, these observations suggest an abnormally  
444 cold and, therefore, wide megathrust seismogenic zone reaching ~65 km depth. It is  
445 worth to further investigate whether these features are inherent to the slow subduction  
446 of slow-spreading oceanic lithosphere in the Atlantic. These results provide a new  
447 framework for advances in operational earthquake locations and future estimation of  
448 seismic hazard in the Eastern Caribbean.

449

## 450 **DATA AND RESOURCES**

451 The optimal 1-D velocity model is made available in the electronic supplement to this  
452 article (Table S1). The relocated earthquake catalogue is available in Table S2. The  
453 Global Centroid Moment Tensor Project database was searched using  
454 [www.globalcmt.org/CMTsearch.html](http://www.globalcmt.org/CMTsearch.html) (last accessed on April 1, 2019). We made figures  
455 using GMT (Wessel and Smalley, 1998). Supplemental content for this article includes  
456 figures showing the quality of earthquake magnitude estimation, the relationship  
457 between station correction and elevation, the comparison of our slab geometry with that  
458 of Slab2.0, and seismicity projected to dense profiles in the central part of the arc.

459

460

## 461 **ACKNOWLEDGEMENTS**

462 This work was funded under NERC grant NE/K010611/1. We thank the “German  
463 Instrument Pool for Amphibian Seismology (DEPAS)”, hosted by the Alfred Wegener  
464 Institute Bremerhaven, for providing the ocean-bottom seismometers and temporary  
465 island seismometers, and UCSD (Scripps) for providing additional ocean-bottom  
466 seismometers. We thank Allison Bent, Zhigang Peng, Hongfeng Yang, and two  
467 anonymous reviewers for their helpful and constructive comments.

468



469 **REFERENCES**

470

471 Allen, R., J. Collier, T. Henstock, A. Stewart, and S. Goes, 2019, A new tectonic model  
472 for the Lesser Antilles: Evidence for a buried arc in the eastern Caribbean, *Geophysical*  
473 *Research Abstract*, 21, EGU2019-7944

474

475 Bakun, W. H., and W. B., Joyner (1984), The ML scale in central California, *Bull.*  
476 *Seismol. Soc. Am.*, 74(5), 1827-1843.

477

478 Bie, L., T. Garth, and A. Rietbrock, 2017, Links between the distribution of intermediate  
479 depth seismicity and structure of the incoming plate in the Lesser Antilles arc, In *AGU*  
480 *Fall Meeting Abstracts*. #T31D-0672

481

482 Abers, G. A., P. E. van Keken, E. A. Kneller, A. Ferris, and J. C. Stachnik (2006), The  
483 thermal structure of subduction zones constrained by seismic imaging: Implications for  
484 slab dehydration and wedge flow, *Earth Planet. Sci. Lett.*, 241(3-4), 387-397.

485

486 Bazin, S., N. Feuillet, C. Duclos, W. Crawford, A. Nercessian, M. Bengoubou-Valérius,  
487 et al., (2010), The 2004–2005 Les Saintes (French West Indies) seismic aftershock  
488 sequence observed with ocean bottom seismometers, *Tectonophysics*, 489(1-4), 91-  
489 103.

490

491 Bird, P. (2003), An updated digital model of plate boundaries, *Geochem. Geophys.*  
492 *Geosyst.*, 4(3), 1027, doi:10.1029/2001GC000252.

493

494 Boynton, C. H., G. K. Westbrook, M. H. P. Bott, and R. E. Long (1979), A seismic  
495 refraction investigation of crustal structure beneath the Lesser Antilles island arc,  
496 *Geophys. J. R. Astron. Soc.*, 58, 371–393.

497

498 Chang, Y., L. M. Warren, and G. A. Prieto (2017), Precise Locations for Intermediate-  
499 Depth Earthquakes in the Cauca Cluster, Colombia, *Bull. Seismol. Soc. Am.*, 107(6),  
500 2649-2663.

501

502 Delouis, B., and D. Legrand (2007), Mw 7.8 Tarapaca intermediate depth earthquake of  
503 13 June 2005 (northern Chile): Fault plane identification and slip distribution by  
504 waveform inversion, *Geophys. Res. Lett.*, 34(1).

505

506 DeMets, C., R. G. Gordon, and D. F. Argus (2010), Geologically current plate motions,  
507 *Geophys. J. Int.*, 181, 1–80.

508

509 Dorel, J. (1981), Seismicity and seismic gap in the Lesser Antilles arc and earthquake  
510 hazard in Guadeloupe, *Geophys. J. R. Astron. Soc.*, 67(3), 679-695.

511

512 Eberhart-Phillips, D. (1990), Three-dimensional P and S velocity structure in the  
513 Coalinga region, California. *J. Geophys. Res.*, 95(B10), 15343-15363.

514

515 Escartín, J., D. K. Smith, J. Cann, H. Schouten, C. H. Langmuir, and S. Escrig (2008),  
516 Central role of detachment faults in accretion of slow-spreading oceanic  
517 lithosphere, *Nature*, 455(7214), 790.  
518

519 Feuillet, N., F. Beauducel, and P. Tapponnier (2011), Tectonic context of moderate to  
520 large historical earthquakes in the Lesser Antilles and mechanical coupling with  
521 volcanoes, *J. Geophys. Res.*, 116(B10), doi:10.1029/2011JB008443  
522

523 Garth, T., and A. Rietbrock (2014), Downdip velocity changes in subducted oceanic  
524 crust beneath Northern Japan-insights from guided waves, *Geophys. J. Int.*, 198(3),  
525 1342-1358. doi:10.1093/gji/ggu206  
526

527 González, O., V. Clouard, and J. Zahradnik (2017), Moment tensor solutions along the  
528 central Lesser Antilles using regional broadband stations, *Tectonophysics*, 717, 214-  
529 225.  
530

531 González, O., V. Clouard, S. Tait, and G. F. Panza (2018), S-wave velocities of the  
532 lithosphere-asthenosphere system in the Lesser Antilles from the joint inversion of  
533 surface wave dispersion and receiver function analysis, *Tectonophysics*, 734, 1-15.  
534

535 Halpaap, F., S. Rondenay, A. Perrin, S. Goes, L. Ottemöller, H. Austrheim, R. Shaw,  
536 and T. Eeken (2019), Earthquakes track subduction fluids from slab source to mantle  
537 wedge sink, *Sci. Adv.*, 5(4), DOI: 10.1126/sciadv.aav7369.  
538

539 Harris, C. W., M. S. Miller, and R. W. Porritt (2018), Tomographic Imaging of Slab  
540 Segmentation and Deformation in the Greater Antilles, *Geochem. Geophys. Geosyst.*,  
541

542 Hayes, G. P., D. E. McNamara, L. Seidman, and J. Roger (2013), Quantifying potential  
543 earthquake and tsunami hazard in the Lesser Antilles subduction zone of the Caribbean  
544 region, *Geophys. J. Int.*, 196(1), 510-521.  
545

546 Hayes, G. P., G. L. Moore, D. E. Portner, M. Hearne, H. Flamme, M. Furtney, and G. M.  
547 Smoczyk (2018), Slab2, a comprehensive subduction zone geometry  
548 model, *Science*, 362(6410), 58-61.  
549

550 Heuret, A., C. P. Conrad, F. Funiciello, S. Lallemand, and L. Sandri (2012), Relation  
551 between subduction megathrust earthquakes, trench sediment thickness and upper  
552 plate strain, *Geophys. Res. Lett.*, 39(5).  
553

554 Heuret, A., S. Lallemand, F. Funiciello, C. Piromallo, and C. Faccenna (2011), Physical  
555 characteristics of subduction interface type seismogenic zones revisited, *Geochem.*  
556 *Geophys. Geosyst.*, 12(1).  
557

558 Hicks, S., A. Rietbrock, I. Ryder, C. Lee, and M. Miller (2004), Anatomy of a megathrust:  
559 The 2010 M8.8 Maule, Chile earthquake rupture zone imaged using seismic  
560 tomography, *Earth Planet. Sci. Lett.*, 405, 142-155, doi.org/10.1016/j.epsl.2014.08.028

561  
562 Husen, S., E. Kissling, E. Flueh, and G. Asch (1999), Accurate hypocentre  
563 determination in the seismogenic zone of the subducting Nazca Plate in northern Chile  
564 using a combined on/offshore network, *Geophys. J. Int.*, 138(3), 687-701.  
565  
566 Iyer, K., B. Jamtveit, J. Mathiesen, A. Malthe-Sørensen, and J. Feder (2008),  
567 Reaction-assisted hierarchical fracturing during serpentinization, *Earth Planet. Sci. Lett.*,  
568 267(3-4), 503-516.  
569  
570 Kennett B. L. N., and E. R. Engdahl (1991), Travel times for global earthquake location  
571 and phase association, *Geophys. J. Int.*, 105, 429-465.  
572  
573 Kissling, E., W. L. Ellsworth, D. Eberhart-Phillips, and U. Kradolfer (1994), Initial  
574 reference models in local earthquake tomography, *J. Geophys. Res.*, 99, 19,635–  
575 19,646, doi:10.1029/93JB03138.  
576  
577 Kissling, E. (1988), Geotomography with local earthquake data, *Rev. Geophys.*, 26(4),  
578 659-698.  
579  
580 Laigle, M., A. Hirn, M. Sapin, A. Bécel, P. Charvis, E. Flueh, et al., (2013), Seismic  
581 structure and activity of the north-central Lesser Antilles subduction zone from an  
582 integrated approach: Similarities with the Tohoku forearc, *Tectonophysics*, 603, 1-20.  
583  
584 Lay, T., H. Kanamori, C. J. Ammon, K. D. Koper, A. R. Hutko, L. Ye, H. Yue, and T. M.  
585 Rushing (2012), Depth-varying rupture properties of subduction zone megathrust  
586 faults. *J. Geophys. Res.*, 117(B4311), doi:10.1029/2011JB009133.  
587  
588 López, A. M., S. Stein, T. Dixon, G. Sella, E. Calais, P. Jansma, Weber, and P.  
589 LaFemina (2006), Is there a northern Lesser Antilles forearc block?, *Geophys. Res.*  
590 *Lett.*, 33(7).  
591  
592 McCann, W. R., and L. R. Sykes (1984), Subduction of aseismic ridges beneath the  
593 Caribbean plate: Implications for the tectonics and seismic potential of the northeastern  
594 Caribbean, *J. Geophys. Res.*, 89(B6), 4493-4519.  
595  
596 McKenzie, D., J. Jackson, and K. Priestley (2005), Thermal structure of oceanic and  
597 continental lithosphere, *Earth Planet. Sci. Lett.*, 233(3-4), 337-349.  
598  
599 Nippres, S. E. J., A. Rietbrock, and A. E. Heath (2010), Optimized automatic pickers:  
600 application to the ANCORP data set. *Geophys. J. Int.*, 181(2), 911-925.  
601  
602 Paulatto, M., M. Laigle, A. Galve, P. Charvis, M. Sapin, G. Bayrakci, ... and H. Kopp  
603 (2017), Dehydration of subducting slow-spread oceanic lithosphere in the Lesser  
604 Antilles, *Nat. Comm.*, 8, 15980.  
605

606 Raffaele, R. M. (2011), Seismic structure of subduction zone of the Lesser Antilles, PhD  
607 thesis, University of Catania.  
608

609 Rietbrock, A., I. Ryder, G. Hayes, C. Haberland, D. Comte, S. Roecker, and H. Lyon-  
610 Caen (2012), Aftershock seismicity of the 2010 Maule Mw8.8, Chile, earthquake:  
611 Correlation between co-seismic slip models and aftershock distribution? *Geophys. Res.*  
612 *Lett.*, 39(8). doi:10.1029/2012GL051308.  
613

614 Ruiz, M., A. Galve, T. Monfret, M. Sapin, P. Charvis, M. Laigle, ... and J. Diaz (2013),  
615 Seismic activity offshore Martinique and Dominica islands (Central Lesser Antilles  
616 subduction zone) from temporary onshore and offshore seismic networks,  
617 *Tectonophysics*, 603, 68-78.  
618

619 Goes, S., et al. (2019), Project VoiLA: Volatile Recycling in the Lesser Antilles, *Eos*,  
620 100, <https://doi.org/10.1029/2019EO117309>.  
621

622 Schlaphorst, D., J. M. Kendall, J. S. Collier, J. P. Verdon, J. Blundy, B. Baptie, ... and M.  
623 P. Bouin (2016), Water, oceanic fracture zones and the lubrication of subducting plate  
624 boundaries—insights from seismicity, *Geophys. J. Int.*, 204(3), 1405-1420.  
625

626 Schlaphorst, D., J. M. Kendall, B. Baptie, J. L. Latchman, and S. Tait (2017), Gaps,  
627 tears and seismic anisotropy around the subducting slabs of the Antilles,  
628 *Tectonophysics*, 698, 65-78.  
629

630 Stein, S., J. F. Engeln, D. A. Wiens, R. C. Speed, and K. Fujita (1983), Slow subduction  
631 of old lithosphere in the Lesser Antilles, *Tectonophysics*, 99(2-4), 139-148.  
632

633 Symithe, S., E. Calais, J. B. De Chabaliere, R. Robertson, and M. Higgins (2015),  
634 Current block motions and strain accumulation on active faults in the Caribbean, *J.*  
635 *Geophys. Res.*, 120(5), 3748-3774.  
636

637 Thurber, C. H. (1992), Hypocenter-velocity structure coupling in local earthquake  
638 tomography, *Phys. Earth Planet. In.*, 75(1-3), 55-62.  
639

640 Uchida, N., S. H. Kirby, T. Okada, R. Hino, and A. Hasegawa (2010), Supraslab  
641 earthquake clusters above the subduction plate boundary offshore Sanriku,  
642 northeastern Japan: Seismogenesis in a graveyard of detached seamounts?, *J.*  
643 *Geophys. Res.*, 115(B9).  
644

645 van Benthem, S., R. Govers, W. Spakman, and R. Wortel (2013), Tectonic evolution  
646 and mantle structure of the Caribbean, *J. Geophys. Res.*, 118(6), 3019-3036.  
647

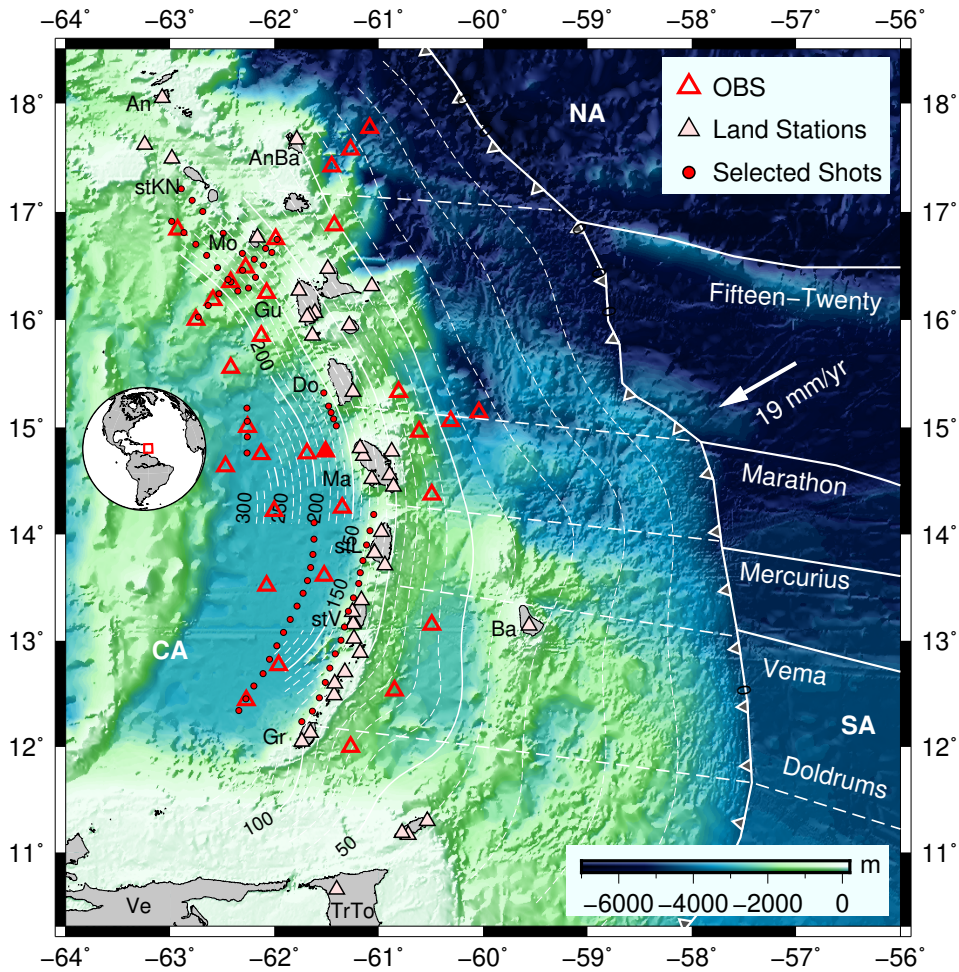
648 Wada, I., and K. Wang (2009), Common depth of slab-mantle decoupling: Reconciling  
649 diversity and uniformity of subduction zones, *Geochem. Geophys. Geosyst.*, 10(10).  
650

651 Wadge, G., and J. B. Shepherd (1984). Segmentation of the Lesser Antilles subduction  
652 zone, *Earth Planet. Sci. Lett.*, 71(2), 297-304.  
653  
654 Weber, J. C., H. Geirsson, J. L. Latchman, K. Shaw, P. La Femina, S. Wdowski, et al.,  
655 (2015), Tectonic inversion in the Caribbean-South American plate boundary: GPS  
656 geodesy, seismology, and tectonics of the Mw 6.7 22 April 1997 Tobago earthquake,  
657 *Tectonics*, 34(6), 1181-1194.  
658  
659 Wessel, P., and R. Smalley (1998). New, improved version of generic mapping tools  
660 released, *Eos Trans. AGU* 79, no. 47, 579-579.  
661  
662 Zhu, G., H. Yang, J. Lin, Z. Zhou, M. Xu, J. Sun, and K. Wan (2019), Along-strike  
663 variation in slab geometry at the southern Mariana subduction zone revealed by  
664 seismicity through ocean bottom seismic experiments, *Geophys. J. Int.*, 218(3), 2122-  
665 2135, doi:10.1093/gji/ggz272.

666 *Lidong Bie*  
667 *Andreas Rietbrock*  
668 *Geophysical Institute, Karlsruhe Institute of Technology, Germany*  
669 *Department of Earth Ocean & Ecological Sciences, University of Liverpool, UK*  
670 [\*l.bie@liv.ac.uk\*](mailto:l.bie@liv.ac.uk)  
671  
672 *Stephen Hicks*  
673 *Robert Allen*  
674 *Jenny Collier*  
675 *Saskia Goes*  
676 *Department of Earth Science & Engineering, Imperial College London, UK*  
677  
678 *Jon Blundy*  
679 *Mike Kendall*  
680 *School of Earth Sciences, University of Bristol, UK*  
681  
682 *Nick Harmon*  
683 *Tim Henstock*  
684 *Kate Rychert*  
685 *Department of Ocean & Earth Sciences, University of Southampton, UK*  
686  
687 *Jon Davidson(Deceased)*  
688 *Colin Macpherson*  
689 *Jeroen van Hunen*  
690 *Department of Earth Sciences, University of Durham, UK*  
691  
692 *Valerie Clouard*  
693 *Stephen Tait*  
694 *Institut de Physique du Globe de Paris, Université Paris Diderot, France*  
695  
696 *Thomas Garth*

697 *Department of Earth Sciences, University of Oxford, UK*  
698  
699 *Lloyd Lynch*  
700 *Richard Robertson*  
701 *Seismic Research Centre, The University of the West Indies, Trinidad and Tobago*  
702  
703 *Frank Krüger*  
704 *Institute of Geosciences, University of Potsdam, Germany*  
705  
706 *Jamie Wilkinson*  
707 *Natural History Museum, London, UK*  
708  
709 *Marjorie Wilson*  
710 *School of Earth & Environment, University of Leeds*  
711

712  
713

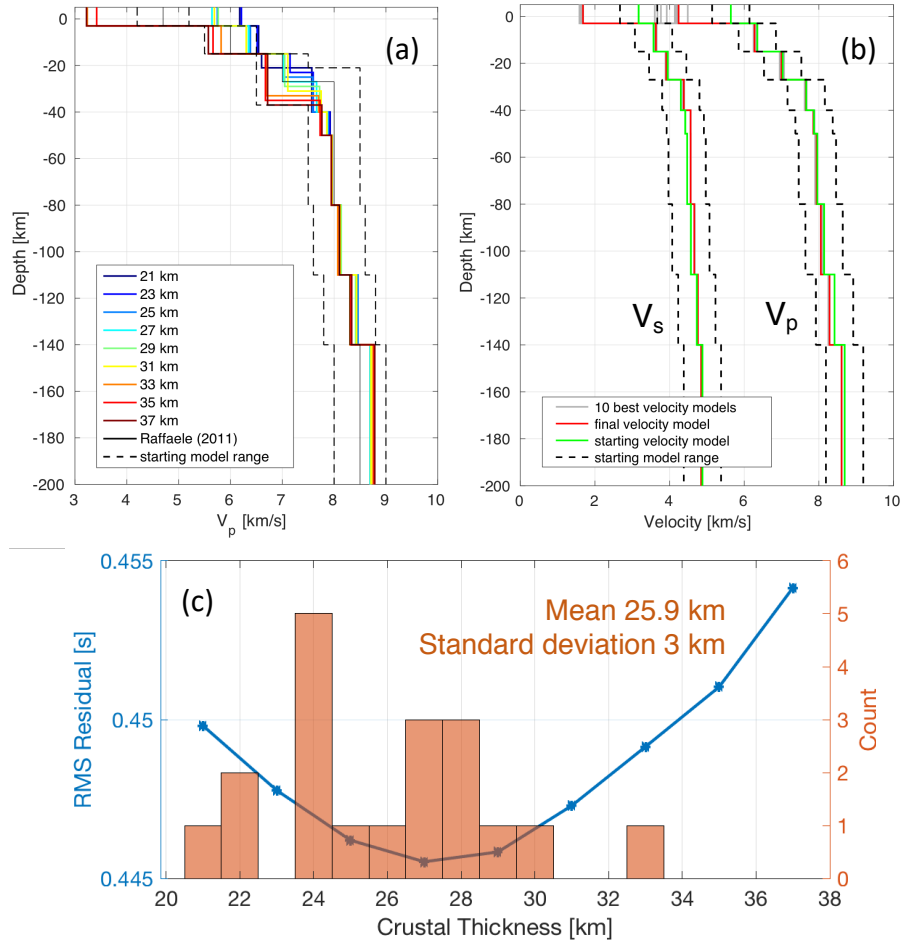


714  
715

716 Figure 1. Tectonic map of the Lesser Antilles subduction zone. Offshore and onshore  
717 seismic stations used in this study are marked by empty red and filled triangles,  
718 respectively. Light white contours depict refined slab geometry from this study.  
719 Reference station in the 1-D velocity inversion is filled by red colour. Red dots in the  
720 back-arc indicate active shots included in the inversion. Details of land stations  
721 incorporated in this study are shown in Figure S1. Inferred fracture zone and spreading-  
722 ridge structures (Schlaphorst *et al.*, 2016) are shown with white lines. CA: Caribbean  
723 Plate; NA: North American Plate; SA: South American Plate. See Figure S1 for details  
724 of island name abbreviations.

725



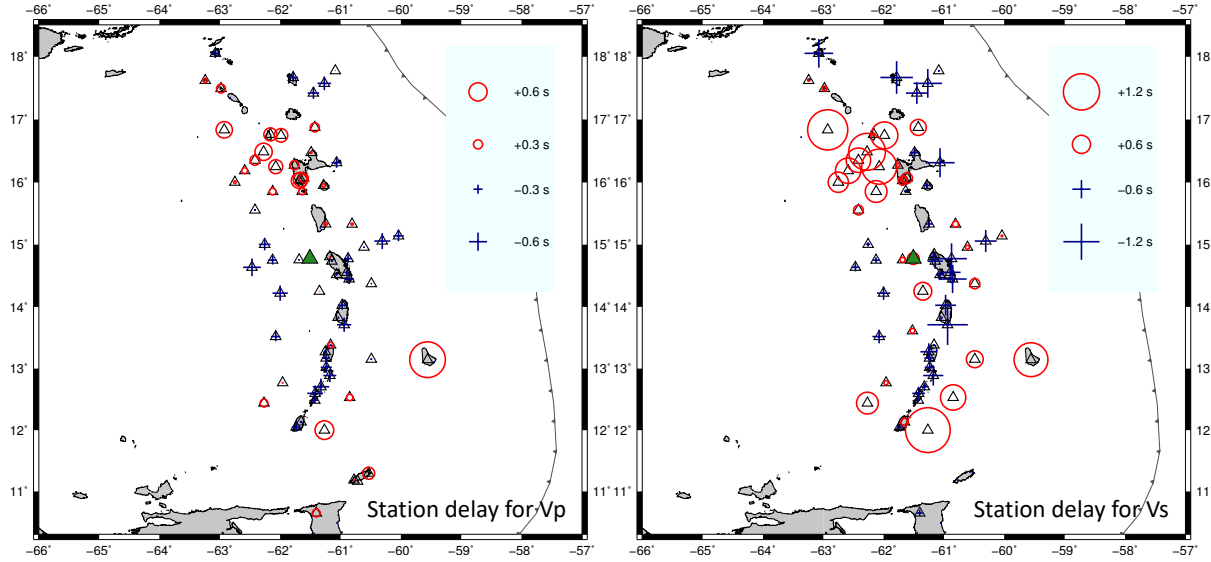


726

727 Figure 2. (a) Best  $v_p$  models for simulations with different starting velocity layer  
 728 configuration. The crustal thickness is varied from 21 km to 37 km, in 2 km increments.

729 (b) Final  $v_p$  and  $v_s$  models for the Lesser Antilles subduction zone. (c) RMS residual  
 730 versus the tested crustal thickness. The minimum RMS misfit is achieved with a crustal  
 731 thickness of 27 km. The bar chart shows the distribution of crustal thickness derived by  
 732 González et al. (2018) from 19 land stations along the arc.

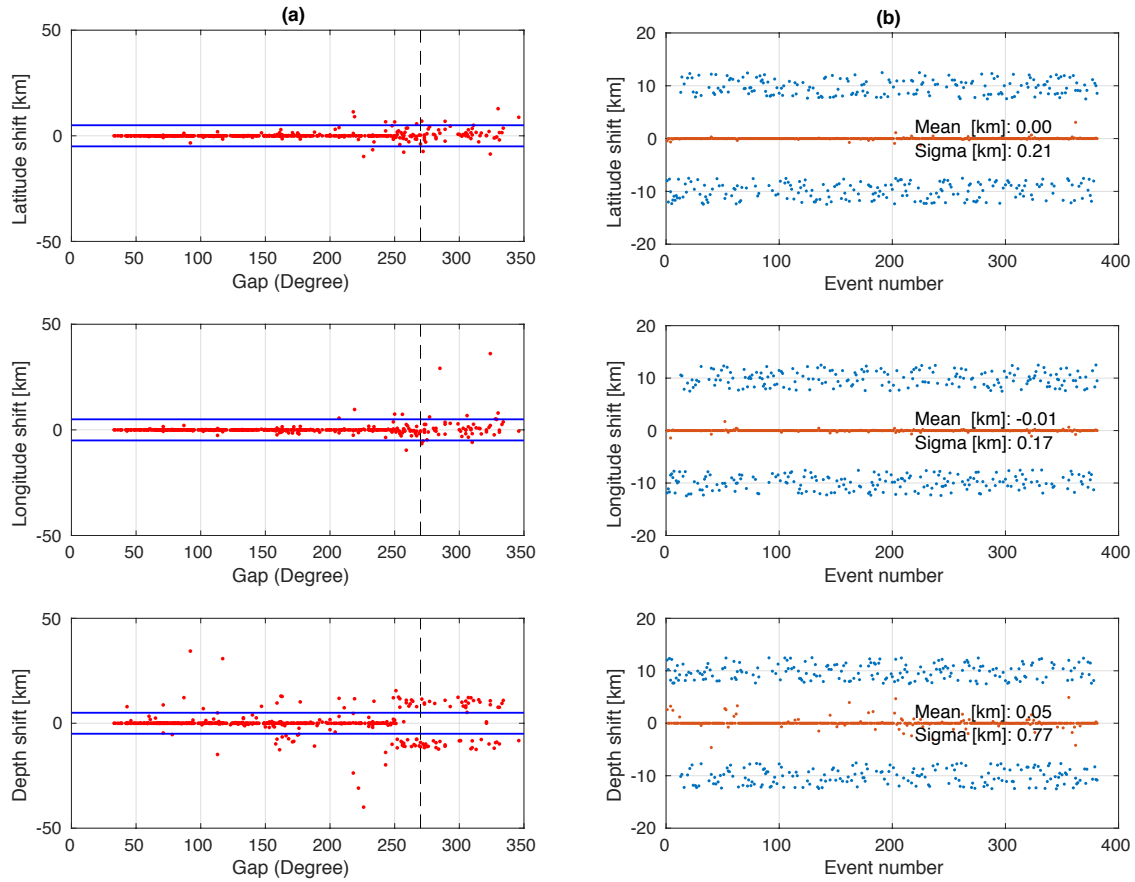
733



734

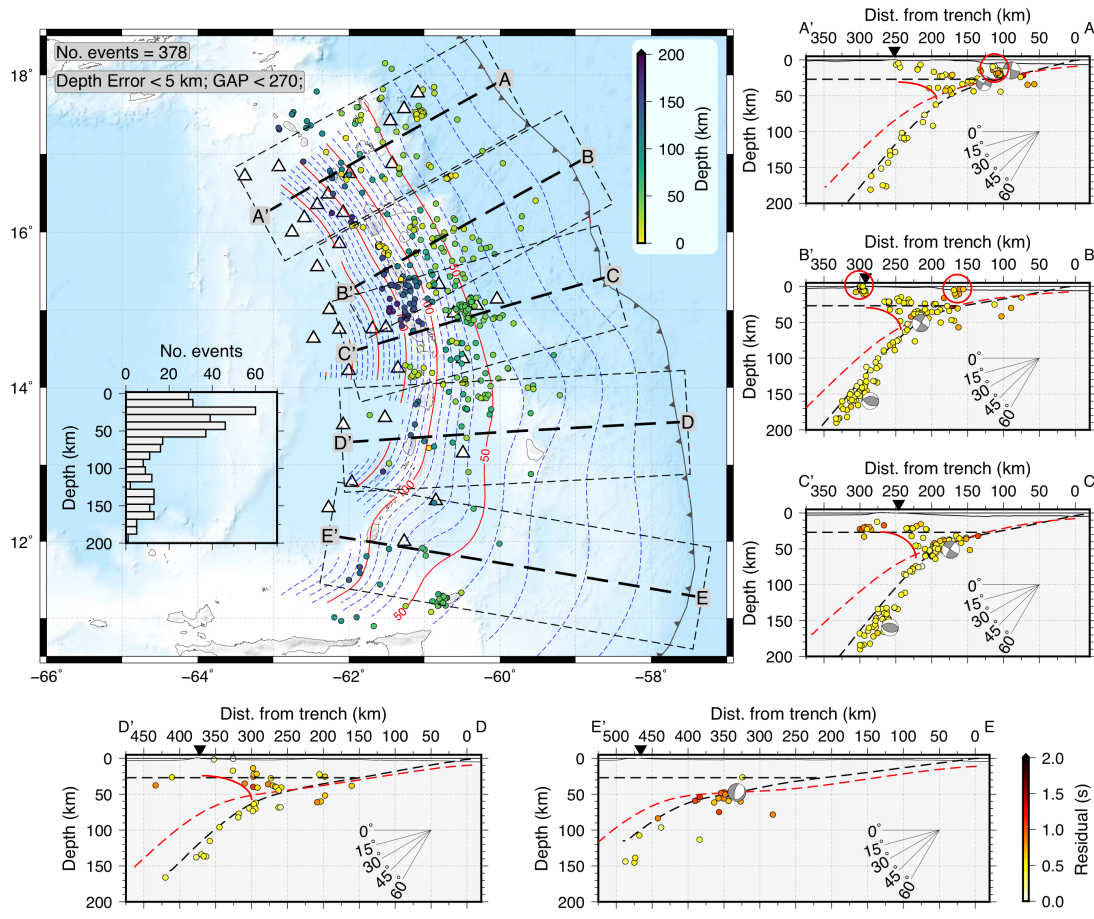
735 Figure 3. Station corrections associated with the velocity model shown in Figure 2b.

736



737

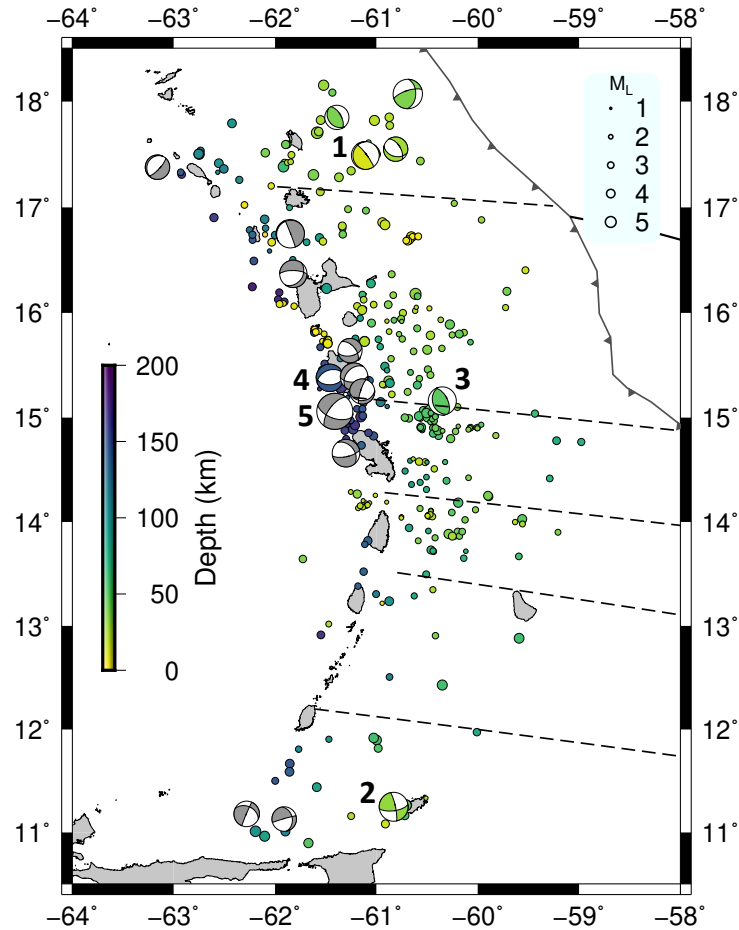
738 Figure 4. Stability test using the velocity model shown in Figure 2b to recover the  
 739 randomly perturbed earthquakes (blue points) in the longitude, latitude and depth  
 740 directions. Those recovered (red points) to be within 5 km (marked as blue line in the  
 741 left panels) from their original locations and having azimuthal gap smaller than 270°  
 742 (black dashed line) are deemed as events with good quality and shown in Figure 5 and  
 743 6. The panels on the right side show the mean and standard deviation of the difference  
 744 between the recovered (red points) and perturbed (blue points) earthquake locations in  
 745 three directions for good quality events.



746  
 747  
 748  
 749  
 750  
 751  
 752  
 753  
 754  
 755  
 756  
 757  
 758  
 759

Figure 5. Distribution of the relocated 378 events coloured by hypocentral depth. The inset shows the number of events versus depth. Triangles are the stations from the VoiLA OBS deployment. Dashed blue and red lines represent the refined slab geometry from this study. Red curve delineates the wedge-shaped mantle corner seismicity. Depth profiles through the regional events comprise earthquakes that are within 75 km perpendicular distance of the labelled lines on the map. In the profiles, earthquakes are coloured by their RMS misfit after the relocation using the best 1-D velocity models from this study. The side hemisphere focal mechanisms from the Global Centroid Moment Tensor Project (see Data and Resources) are plotted. Black dashed curves are from slab model generated in this study, while the red dashed curves are from Slab2.0 (Hayes et al., 2018).

760



761

762 Figure 6. Local seismicity as derived from this study. Focal mechanisms (FM) for events  
763 with GCMT (see Data and Resources) solutions during the period of passive-seismic  
764 experiments are coloured by depth. Focal mechanisms for all historical deep (> 70 km)  
765 normal fault events (at least one slip direction between -145° and -90°) in the GCMT  
766 catalogue and from Gonzalez et al. (2017) are marked in grey. FM 1:  $M_w$  5.7,  
767 2017/04/17; FM 2:  $M_w$  5.9, 2016/12/06; FM 3:  $M_w$  5.8, 2017/02/03; FM 4:  $M_w$  5.6,  
768 2016/10/18; FM 5:  $M_w$  7.4, 2007/11/29.

769